Magnetic properties of nanoparticles in the Bethe-Peierls approximation

Luis G. C. Rego* and Wagner Figueiredo
Departamento de Física, Universidade Federal de Santa Catarina, Florianópolis, SC 88040-900, Brazil
(Received 3 April 2001; published 21 September 2001)

In this work we present a method to calculate the classical magnetic properties of single-domain nanoparticles. Based on the Bethe-Peierls (pair) approximation, we developed a simple system of equations for the classical magnetization of spins at any position within the nanoparticle. Nearest-neighbor pair correlations are treated exactly for Ising spins, and the method can be generalized for various lattice symmetries. The master equation is solved for the Glauber dynamics (single spin flip) in order to obtain the time evolution of the magnetization. The capabilities of the model are demonstrated through nontrivial calculations of hysteresis loops as well as field cooling and zero-field cooling magnetization curves of heterogeneous noninteracting nanoparticles. The present method automatically incorporates temperature and could be adapted to describe an ensemble of interacting nanoparticles.

DOI: 10.1103/PhysRevB.64.144424 PACS number(s): 75.50.Tt, 75.60.−d

I. INTRODUCTION

The properties of magnetic nanoparticles and fine particle assemblies have been attracting the interest of physicists for many decades. Below a critical size such nanoscopic magnetic systems develop properties that cannot be found in macroscopic systems, where the material is divided into domains in order to decrease the magnetostatic energy. Stoner and Wohlfarth[1] laid the theoretical basis, which is widely used nowadays, to describe such low-dimensional systems and predicted effects like superparamagnetism. According to the Stoner-Wohlfarth model, the strong exchange interaction aligns all the particle spins so that the magnetization inside the nanoparticle is assumed to be a uniform field, which rotates coherently due to the presence of an external magnetic field. Despite being a suitable assumption for homogeneous systems, it is not appropriate to describe heterogeneous particles, for instance, formed by regions of localized moments having distinct magnetic character (ferromagnetic, ferrimagnetic, and antiferromagnetic). For such heterogeneous systems the exchange energy plays a central role in determining the magnetization of the nanoparticle.[2–4] Unfortunately, the nontrivial interaction among the spins is responsible for a highly correlated behavior that is very difficult to describe in terms of analytical expressions or exact numerical solutions, for a general case. In addition, the boundary conditions imposed by the finite size of the nanoparticles and surface disorder complicate otherwise simpler solutions for infinite systems.

In most experiments the magnetization due to an ensemble of nanoparticles is the measured parameter. In this case the long-range dipolar interaction is dominant; it produces a collective energy barrier for the magnetization reversal of a nanoparticle and, consequently, sets a new time scale for irreversible processes,[5] the magnetization of independent nanoparticles being experimentally accessible in the limit of very dilute particle ensembles. However, a series of recent experiments, using a micro superconducting quantum interference device (micro-SQUID) technique, have demonstrated the possibility of measuring both the magnetization reversal mechanism and dynamics of individual homogeneous nanoparticles (10–20 nm in diameter) (Ref. 6) and cobalt nanoclusters (3–5 nm in diameter).[7] The formalism presented in this paper should provide a theoretical foundation for experiments made on single (or independent) heterogeneous nanoparticles.

Magnetic systems are well known for developing long-range interactions, especially in the continuous phase transitions, where the correlation length is infinite. Because of that, the calculation of critical exponents requires sophisticated theoretical formalisms such as renormalization group techniques, high-temperature series expansions, or numerical methods such as the Monte Carlo method. On the other hand, away from the critical point, where the correlation length decays exponentially, a mean-field theory may provide a good description of the behavior of the system. Nevertheless, the plain mean-field approach corresponds to one in which there is no correlation between any pair of spins and a given spin interacts with the average magnetization of its neighbors or, equivalently, with an effective mean field produced by all the spins in the system. This simplified approach might fail, however, for nanoparticles having a core with magnetic properties that differ from those of the surface, as in the instance of a ferromagnetic particle coated by a ferrimagnetic or antiferromagnetic layer,[3] caused by oxidation processes, or the case of a disordered surface as well.[4] For these systems the correlations between neighbors are important to establish boundaries between regions of different magnetic properties.

In this work we propose a method to describe the classical magnetic properties of noninteracting nanoparticles. The method takes a further step from the standard mean-field approach and treats the nearest-neighbor pair correlations between spins within the particle explicitly, therefore being capable of describing heterogeneous systems. In spite of being extensively used to calculate the magnetic properties of infinite systems, the Bethe-Peierls (also called pair) approximation has not yet been used to calculate the magnetic properties of nanoparticles. A somewhat similar approach was used to describe the magnetization of Fe quasi-one-dimensional (quasi-1D) clusters,[8] in view of the fact that the results obtained by the Bethe-Peierls approximation agree with the

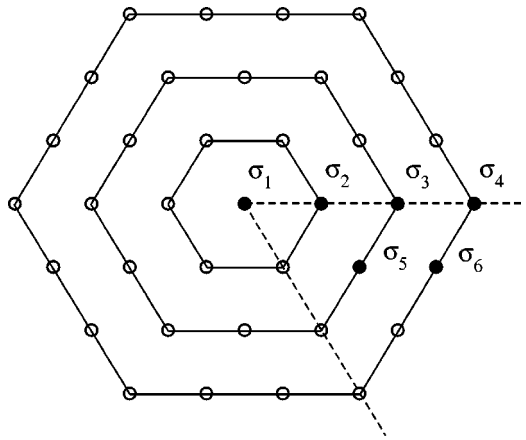

FIG. 1. Schematic representation of an hexagonal nanoparticle exhibiting three shells of spins (small circles). The representative spins that compose the set of equations for this particle are represented by solid circles. The dashed lines evidence the sixfold symmetry.

Ising solution for 1D systems.[9] In the following the details of the model and the formalism are presented. Then, in the remainder of the paper, it is shown that the model accounts for many of the properties of magnetic nanoparticle systems.

II. THEORY

At first, consider a 2D array of Ising spins in a hexagonal lattice, as depicted in Fig. 1 for a structure made up of three shells. A similar model system could be used to describe the properties of single-crystalline disks with hexagonal contour, such as 10–20 nm BaFeCoTiO nanoparticles whose magnetization reversal has been measured.[6] We note that the formalism applies equally well for any 2D lattice and can be extended to 3D lattices as well. Taking advantage of the sixfold rotational symmetry of the lattice, we need to consider only a small subset of spins (marked $\sigma_1-\sigma_6$ by solid circles in Fig. 1) to provide the magnetization of the whole particle. Each of the spin sites, which stand for the atomic moments in the nanoparticle, are described by Ising spin variables that take on values $\sigma_i=\pm 1$. The nanoparticle is assumed to be very small, so that it constitutes a monodomain. In addition, according to experimental results,[6] an uniaxial anisotropy is implicit in the model, with the easy axis coinciding with the Ising spin direction. Therefore the energy of the system is written as

$$\mathcal{H}=-\sum_{\langle i,j\rangle} J_{ij}\sigma_i\sigma_j-H\sum_i \sigma_i, \tag{1}$$

where only the exchange coupling between nearest neighbors is considered, with J_{ij} as the exchange coupling constant and H is the applied magnetic field.

Having defined the relevant spins that describe the system we start by writing the dynamical equations for the average spin magnetizations,

$$m_i(t)=\langle\sigma_i\rangle=\sum_\sigma \sigma_i P(\sigma,t), \tag{2}$$

and the pair correlation functions

$$r_{ij}(t)=\langle\sigma_i\sigma_j\rangle=\sum_\sigma \sigma_i\sigma_j P(\sigma,t), \tag{3}$$

where the index i, as well as j, designates a spin site and the sum over σ accounts for all the spin configurations. Since we restrict our model to take into account only pair correlations, the probability of a given spin configuration is written as[10]

$$P(\sigma,t)=\frac{1}{2^N}\left\{1+\sum_i \sigma_i m_i(t)+\sum_{i<j}\sigma_i\sigma_j r_{ij}(t)\right\}, \tag{4}$$

where N is the total number of spins.

The time evolution of the system is obtained by means of the master equation for the probabilities,

$$\frac{dP(\sigma,t)}{dt}=\sum_{\sigma'}\{P(\sigma',t)w(\sigma',\sigma)-P(\sigma,t)w(\sigma,\sigma')\}, \tag{5}$$

with $w(\sigma',\sigma)$ as the transition probability per unit time from the spin configuration σ' to configuration σ. Here we assume that the dynamics of the system is governed by single-spin-flip transitions, which can be mathematically described by the Glauber formalism[10]

$$w_i(\sigma_i)=\frac{1}{2\tau}\{1-\sigma_i\gamma\}, \tag{6}$$

with

$$\gamma(J,\beta,H)=\tanh\left[\left(\sum_j J_{ij}\sigma_j+H\right)/k_BT\right]\equiv\tanh(\Delta_i), \tag{7}$$

where k_B is the Boltzmann constant, T is the absolute temperature, and τ is the relaxation time for a single spin. This dynamical rule is chosen so that the transition probabilities $w_i(\sigma_i)$ depend on the spin value of σ_i as well as on the values of its nearest neighbors.

Using Eqs. (5)–(7) we obtain after some algebraic manipulation the dynamical equations for $m_i(t)$ and $r_{ij}(t)$:

$$\frac{dm_i(t)}{dt}=-\frac{1}{\tau}\left\{m_i(t)-\sum_\sigma \tanh(\Delta_i)P_i(\sigma,t)\right\}, \tag{8}$$

$$\frac{dr_{ij}(t)}{dt}=-\frac{1}{\tau}\left\{2r_{ij}(t)-\sum_\sigma[\sigma_i\tanh(\Delta_j)+\sigma_j\tanh(\Delta_i)]P_{ij}(\sigma,t)\right\}. \tag{9}$$

In principle, our task is to integrate these equations to obtain the time evolution of the variables of interest. Within the Bethe-Peierls approximation,[11] we assume that only the correlations between pairs of nearest neighbors are nonzero and write the following equation for $P_i(\sigma)$:

$$P_i(\sigma)=\frac{\prod_{\alpha}^{N_i} P(\sigma_i,\sigma_\alpha)}{P^{N_i-1}(\sigma_i)}, \tag{10}$$

where N_i is the coordination number of the lattice site i and for $P_{ij}(\sigma)$,

$$P_{ij}(\sigma)=\frac{P(\sigma_i,\sigma_j)}{P^{N_i-1}(\sigma_i)P^{N_j-1}(\sigma_j)}\prod_{\alpha}^{N_i} P(\sigma_i,\sigma_\alpha)\prod_{\beta}^{N_j} P(\sigma_i,\sigma_\beta). \tag{11}$$

It is important to notice that N_i is different for the surface spins. $P(\sigma_i)$ and $P(\sigma_i,\sigma_j)$ are obtained from expression (4) taking as nonzero only the nearest-neighbor correlation functions:

$$P(\sigma_i)=\frac{1}{2}(1+m_i\sigma_i), \tag{12}$$

$$P(\sigma_i,\sigma_j)=\frac{1}{4}(1+m_i\sigma_i+m_j\sigma_j+r_{ij}\sigma_i\sigma_j). \tag{13}$$

Substituting expressions (10) and (11) into the dynamical equations (8) and (9) yields, after a straightforward manipulation, a closed system of equations for the spin magnetizations $[m_i(t)]$ and nearest-neighbor pair correlation functions $[r_{ij}(t)]$ that can be solved numerically,

$$\tau\frac{dm_i(t)}{dt}+m_i(t)=\sum_{k=0}^{N_i}\left\{\frac{t_{6-k}}{x_i^5}\hat{\mathcal{V}}^k Z_i(\{N_i\})+\frac{t_k}{y_i^5}\hat{\mathcal{U}}^k W_i(\{N_i\})\right\}, \tag{14}$$

$$\tau\frac{dr_{ij}(t)}{dt}+2r_{ij}(t)=[\xi_i]_j+[\xi_j]_i, \tag{15}$$

with

$$[\xi_i]_j=\sum_{k=0}^{N_j-1}\{[z_i]_j t_{6-k}-[v_i]_j t_{5-k}\}\frac{\hat{\mathcal{V}}^k Z_j(\{N_j\})}{x_j^5}+\sum_{k=0}^{N_j-1}\{[u_i]_j t_{1+k}-[w_i]_j t_k\}\frac{\hat{\mathcal{U}}^k W_j(\{N_j\})}{y_j^5}, \tag{16}$$

and $[\xi_j]_i$ obtained by the simple exchange of the indices i and j in Eq. (16). Refer to the Appendix for a definition of the symbols. We also define the products

$$Z_j(\{N_j\})=\prod_{\alpha}^{N_j}[z_\alpha]_j, \tag{17}$$

$$W_j(\{N_j\})=\prod_{\alpha}^{N_j}[w_\alpha]_j, \tag{18}$$

upon which act the operators

$$\hat{\mathcal{V}}^k\equiv\sum_{\alpha_1<\cdots<\alpha_k}\frac{[v_{\alpha_1}]_j\cdots[v_{\alpha_k}]_j}{[z_{\alpha_1}]_j\cdots[z_{\alpha_k}]_j}, \tag{19}$$

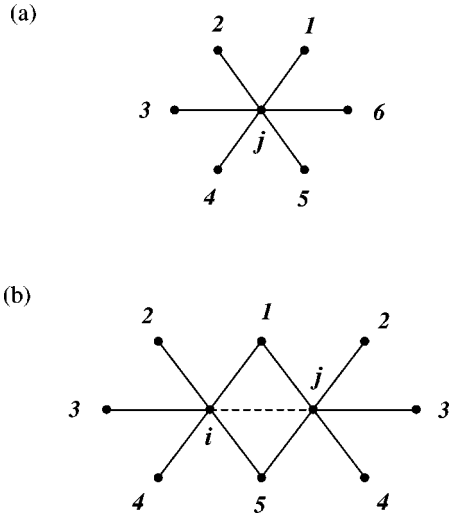

FIG. 2. (a) A cluster formed by spin σ_j and its six nearest neighbors. (b) A cluster formed by the pair $\sigma_i\sigma_j$ and their nearest neighbors.

$$\hat{\mathcal{U}}^k\equiv\sum_{\alpha_1<\cdots<\alpha_k}\frac{[u_{\alpha_1}]_j\cdots[u_{\alpha_k}]_j}{[w_{\alpha_1}]_j\cdots[w_{\alpha_k}]_j}, \tag{20}$$

which generate all the possible configurations of the cluster. In the case of Eq. (14) the independent indices α_k stand for all the nearest neighbors ($1\leqslant\alpha_k\leqslant 6$) of a given spin σ_j, as depicted in Fig. 2(a). When calculating the pair correlations $r_{ij}=\langle\sigma_i\sigma_j\rangle$, $1\leqslant\alpha_k\leqslant 5$, to avoid counting the pair twice, as shown in Fig. 2(b) for spins σ_i and σ_j. For $k=0$, $\hat{\mathcal{V}}^0=1$ and $\hat{\mathcal{U}}^0=1$. The parameter t_k is related to the transition rate of a spin:

$$t_k=\tanh\left(\frac{2J(k-3)+H}{k_BT}\right). \tag{21}$$

The results comprehending Eqs. (14)–(20) correspond to the case $J_{ij}=J$. To account for the more complex case of different J_{ij} in heterogeneous nanoparticles $\hat{\mathcal{V}}^k$ and $\hat{\mathcal{U}}^k$ have to be modified to incorporate a generalized parameter t_k. This is done in the Appendix.

III. RESULTS AND DISCUSSIONS

In this section we describe the properties of the model and show that it accounts for many of the phenomena presented by magnetic nanoparticle systems.

We start by discussing the properties of the hysteresis of noninteracting homogeneous ferromagnetic nanoparticles, as yielded by the present model. For this purpose consider Fig. 3(a) where hysteresis loops for three different nanoparticle sizes $R=1$, 2, and 11 are shown. R is the number of shells and can be associated with the radius of the nanoparticle. We define the total magnetization of the nanoparticle $M\equiv\Sigma_i m_i(t)/N$, where the sum runs over all the spins of the nanoparticle (N). The smallest nanoparticle ($R=1$) has vanishing coercive field and its magnetization is well fitted by a Langevin function, whereas the bigger particles ($R=2-11$)

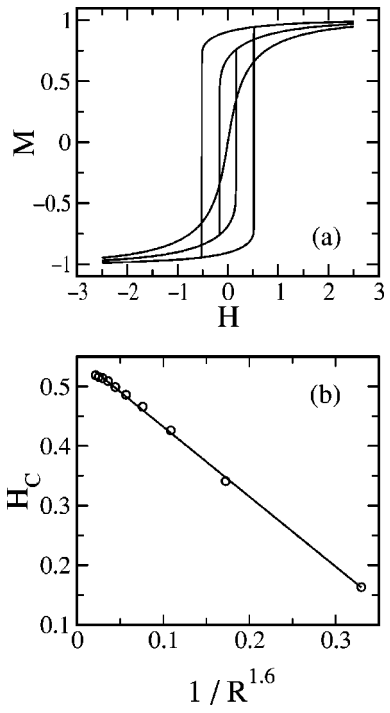

FIG. 3. (a) Hysteresis loops for various nanoparticle sizes: $R=1$, 2, and 11. The reduced temperature is $T=3J/k_B$, where $J=1$ is the exchange coupling constant and k_B is the Boltzmann constant. (b) The coercive field (H_C in units of J) plotted as a function of $R^{-1.6}$. From right to left, the dots correspond to $R=2,3,\ldots,11$ and the straight line results from a linear fit to the data.

exhibit typical hysteresis loops of ferromagnetic nanoparticles. Figure 3(b) shows the dependence of the coercive field (H_C) on the number of shells of the nanoparticle, by plotting H_C as a function of $R^{-1.6}$, for the reduced temperature $k_BT=3J$. This graph demonstrates that the functional relation $H_C \sim R^{-1.6}$ fits very well the results of our calculations for nanoparticles of size $2 \leqslant R \leqslant 10$, with the exception of the $R=1$ and $R=11$ cases. The former is in the superparamagnetic regime, as indicated by Fig. 3(a), whereas the last already starts to behave as an infinite system. The same behavior exhibited by H_C in Fig. 3(b) is obtained for the reduced temperature $k_BT=1.5J$. According to our calculations, for $R>10$ the Curie temperature (T_C) of the nanoparticle approaches the T_C of an infinite cubic system, as yielded by the Bethe-Peierls relation $\coth[J/k_BT_C]=5$.[9] Calculations for a square lattice showed that $H_C \sim L^{-1.5}$ for small clusters, where L stands for its lateral dimension. Finally, we point out that the mechanism of magnetization reversal that takes place in our nanoparticle is not entirely coherent. Because of their smaller coordination number, the average magnetization (m_i) of the outside spin shells decreases by the action of the reverse field H, consequently also decreasing the magnetization of their neighboring shells and creating a nonuniform magnetization profile. Eventually, when H reaches H_C, all spins flip together. This process should be responsible for easier magnetization rotation and lower switching fields than those given by the Stoner-Wohlfarth model.

In the remainder of this section we consider the properties

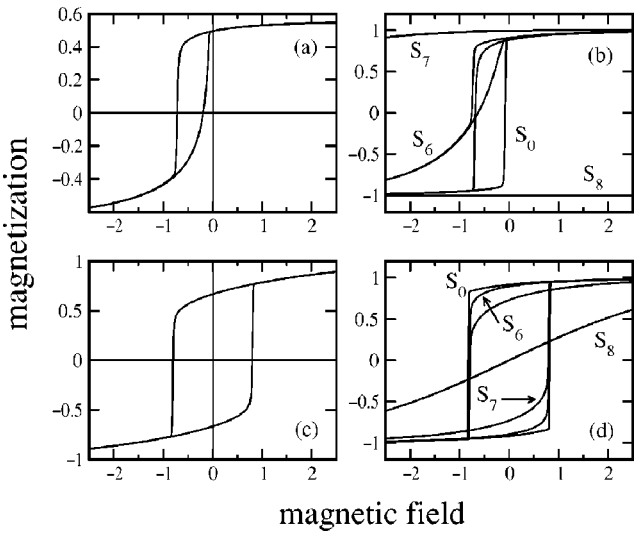

FIG. 4. (a) Hysteresis loop for a nanoparticle of radius $R=8$. Here $J_C=1$ for $R \leqslant 7$, $J_S=5$ in the surface $R=8$, and $J_{C\text{-}S}=-4$ couples the core and surface regions. (b) Individual magnetization curves for the center spin (S_0), a spin in the sixth shell (S_6), a spin in the seventh shell (S_7), and a spin in the surface shell (S_8). (c) Same parameters as in (a) using a simple mean-field approach, the exchange shift disappears. (d) Same as (b) for a simple mean field. The reduced temperature is $k_BT=3.5J_C$ for all curves.

of heterogeneous nanoparticles, which are more complex systems, e.g., consisting of ferromagnetic and antiferromagnetic (or ferrimagnetic) regions coupled with each other. Examples of such systems are oxide-coated cobalt (Co) or iron (Fe) nanoparticles,[3] among many others that exhibit the exchange anisotropy effect.[13,14] When cooled in the presence of an external magnetic field the soft ferromagnetic core of the particle aligns with the applied field but its outer antiferromagnetic (AF) surface gets ordered only when the temperature of the system is lower than T_N (Néel temperature).[12] The coupling of the ferromagnetic core with the antiferromagnetic surface therefore produces a unidirectional exchange anisotropy that shifts the hysteresis loop to higher or lower magnetic fields, depending on their mutual orientation. Having said that, consider an eight-shell nanoparticle with the following characteristics: the exchange interactions in the core ($R=0-7$) are given by the coupling parameter $J_C=1$, the outmost shell ($R=8$) is also ferromagnetic with an exchange constant $J_S=5$, and the coupling between the $R=7$ and $R=8$ shells is due to an antiferromagnetic exchange constant $J_{C\text{-}S}=-4$. The hysteresis we obtain with our formalism is shown in Fig. 4(a), which presents a clear exchange shift. Figure 4(b) shows the magnetization curves of individual spins within the nanoparticle: in the center of the nanoparticle (S_0), in the sixth shell (S_6), in the seventh shell (S_7), and in the surface shell (S_8). As evidenced by this graph, the surface shell and the layer just below it are locked in a very stable AF configuration, whereas the average magnetization of the inner ferromagnetic shells varies gradually towards the center of the particle. For the sake of comparison, we have also calculated the hysteresis for the same system, but using a simple mean-field approach, whose results

are shown in Figs. 4(c) and 4(d). For the standard mean-field equations each spin experiences only an effective field that can be seen as an average interaction with all the other spins and, consequently, the exchange shift disappears. Looking at the individual spin magnetizations [Fig. 4(d)] it is evident that there is no correlation between the surface and core domains.

Another important experimental technique used to investigate the properties of magnetic nanoparticles is the field cooling (FC) and zero-field cooling (ZFC) magnetization measurements. For an ensemble of noninteracting homogeneous particles the blocking temperature (T_B) is related to the magnetic anisotropy constant and the volume of the nanoparticle.[12] For a system of interacting nanoparticles see Ref. 5. The blocking temperature, where the maximum of the ZFC curve occurs, indicates the point in which the thermal energy is comparable to the average anisotropy barrier in the nanoparticles, and beyond it the magnetization decreases with temperature. In the following we show a deblocking behavior that is caused only by the exchange interaction between antiferromagnetic and ferromagnetic regions in a single nanoparticle. For that purpose consider a six-shell nanoparticle whose core is predominantly AF, $J_C=-0.5J_0$ for $R=0-5$, with a ferromagnetic surface, $J_S=2J_0$ for $R=6$, which is ferromagnetically coupled with the core, $J_{CS}=1J_0$ between $R=5$ and $R=6$. The energy parameter is $J_0=1$ and the time taken to sweep over the whole temperature interval is $t_s=10^4\tau$, with τ appearing in Eqs. (8) and (9). The calculations were performed in accordance with the standard FC-ZFC experimental practice.[15] The obtained FC (solid line) and ZFC (dashed line) magnetization curves are shown in Figs. 5(a)–5(f) as a function of the reduced temperature, for values of the applied field that vary from $H=0.05|J_0|$ to $H=0.0001|J_0|$. Here M is the normalized magnetization of the entire nanoparticle, as previously defined. Because it corresponds to a single particle, T_B is sharply marked and does not exhibit the characteristic dispersion caused by the size distribution of the particles. According to our calculations, T_B is not strongly dependent on J_C; however, it does depend on J_{SC} and J_S. Figure 5 shows that the blocking temperature occurs just about the range $J_{CS}\leqslant k_BT_B\leqslant J_S$, which has been confirmed in calculations for different nanoparticle parameters (size, exchange constant, and t_s). Despite being observed to take place for nanoparticles of different sizes, the blocking temperature effect is very sensitive to the relative strengths between the ferromagnetic and antiferromagnetic exchange constants. For clarity, Fig. 6 displays the relation between the average magnitude of the energies associated with the parallel spin alignment (U_F+U_H) and antiparallel spin alignment (U_{AF}) configurations within the particle,

$$U_F=\left\langle \sum_{\langle i,j\rangle} J_S\sigma_i\sigma_j+\sum_{\langle k,l\rangle} J_{CS}\sigma_k\sigma_l \right\rangle = J_S\sum_{\langle i,j\rangle} r_{ij}+J_{CS}\sum_{\langle k,l\rangle} r_{kl}, \tag{22}$$

$$U_H=H\left\langle \sum_i \sigma_i \right\rangle = H\sum_i m_i, \tag{23}$$

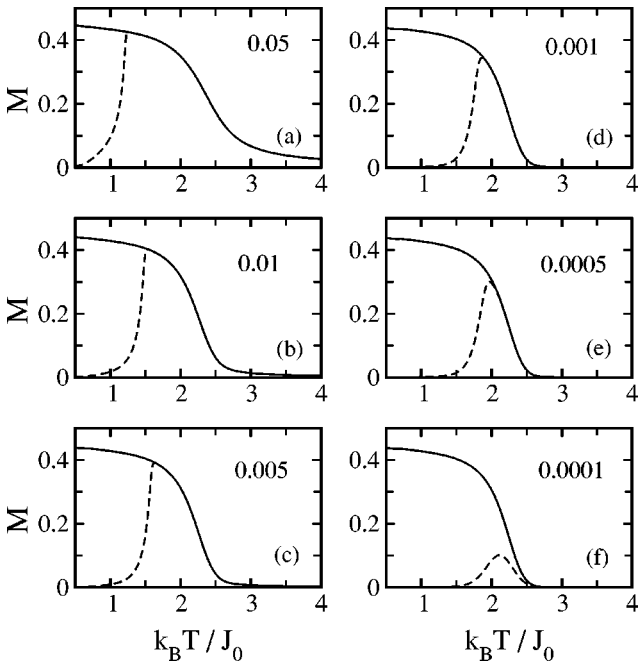

FIG. 5. FC (solid) and ZFC (dashed) curves of the total normalized magnetization (M) as a function of the reduced temperature k_BT/J_0. Different values for the applied magnetic field are considered, from $H=0.05|J_0|$ in (a) through $H=0.0001|J_0|$ in (f), as indicated in the figures. The nanoparticle consists of $R=6$ shells, with an AF core ($J_C=-0.5J_0$, for $0\leqslant R\leqslant 5$), a ferromagnetic surface ($J_S=2J_0$ within $R=6$), and a ferromagnetic coupling between core and surface ($J_{CS}=1J_0$, between $R=5$ and $R=6$).

$$U_{AF}=\left\langle \sum_{\langle i,j\rangle} J_C\sigma_i\sigma_j \right\rangle = J_C\sum_{\langle i,j\rangle} r_{ij}, \tag{24}$$

in terms of which we define the differential exchange energy $\Delta_{XC}\equiv(U_F+U_H-U_{AF})/(U_F+U_H+U_{AF})$. Solid and dashed lines represent FC and ZFC processes, respectively, and the arrows indicate their dynamics. The contribution of the U_H term to the total energy of the nanoparticle is very small; however, it is responsible for the deblocking behavior at T_B. At the high-temperature regime the average exchange energy is nonzero, because of a remaining finite short-range correlation between nearest-neighbor pairs. Most of the energy is due to the ferromagnetic ordering. During the ZFC (dashed

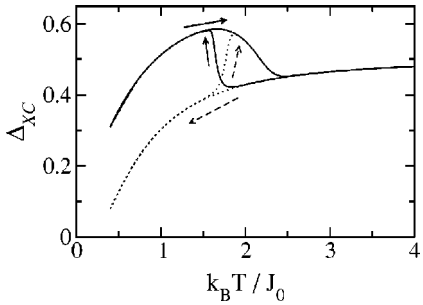

FIG. 6. Differential exchange energy $\Delta_{XC}\equiv(U_F+U_H-U_{AF})/(U_F+U_H+U_{AF})$ as a function of the reduced temperature k_BT/J_0. The applied field is $H=0.001|J_0|$.

line) the AF core overwhelms the ferromagnetic surface and forces the magnetization of the whole nanoparticle to vanish. Then, in the subsequent heating, even a very small applied field is enough to trigger the alignment of the ferromagnetic surface, which is evidenced by the relative increase of the ferromagnetic energy. On the other hand, during the FC process the applied field is able to magnetize the nanoparticle at higher temperatures, before the AF correlations of the core become too strong. Therefore, the interplay between AF and F exchange energies gives rise to the hysteresis in temperature that we observe in the FC-ZFC calculations.

IV. CONCLUSIONS

We have developed an approach to calculate the classical magnetic properties of single-domain nanoparticles. Treating the nearest-neighbor pair correlation functions explicitly we were able to obtain a simple set of equations for the magnetization at any point in the particle. In addition, Eqs. (14) and (15) can also account for the inclusion of interactions between next-nearest neighbors in a straightforward manner, by incorporating the corresponding J_{ij} into the operators (A5) and (A6) and increasing the coordination number N_j of each spin. The method can be applied to different lattice geometries and extended to 3D systems. The formalism treats correctly the short-range correlations that arise in heterogeneous nanoparticles, which have regions of different magnetic properties, e.g., oxidized ferromagnetic particles. Such spin correlations were evidenced by the observation of the exchange shift in hysteresis loops and by the blocking-deblocking effect in the FC-ZFC calculations.

ACKNOWLEDGMENTS

The authors thank M.L. Sartorelli for fruitful discussions. Financial support for this work was provided by CNPq-Brazil.

APPENDIX

Here we define some of the notation used in Sec. II. Based on Eq. (4), Eq. (14), and (15) are written out in terms of the following simple functions:

$$x_i=\frac{1+m_i}{2}, \quad y_i=\frac{1-m_i}{2}, \tag{A1}$$

$$[z_i]_j=\frac{1+m_i+m_j+r_{ij}}{4},[w_i]_j=\frac{1-m_i-m_j+r_{ij}}{4}, \tag{A2}$$

$$[v_i]_j=\frac{1-m_i+m_j-r_{ij}}{4},[u_i]_j=\frac{1+m_i-m_j-r_{ij}}{4}, \tag{A3}$$

where $[z_i]_j=[z_j]_i$ and $[w_i]_j=[w_j]_i$. As already mentioned in the main text, the parameter t_k in Eqs. (14) and (15) is related to the transition rate of a spin,

$$t_k=\tanh\left(\frac{2J(k-3)+H}{k_BT}\right), \tag{A4}$$

for $J_{ij}=J$ and in accordance with the definitions given in the main text. For the case of general exchange constants (J_{ij}), the term t_k must be generalized and incorporated into the operators $\hat{\mathcal{V}}^k$ and $\hat{\mathcal{U}}^k$,

$$\hat{\mathcal{V}}^k\equiv\sum_{\alpha_1<\cdots<\alpha_k}\frac{[v_{\alpha_1}]_j\cdots[v_{\alpha_k}]_j}{[z_{\alpha_1}]_j\cdots[z_{\alpha_k}]_j}\times\tanh\left(\frac{\sum_{\beta=1}^{N_j}J_{\beta j}-2(J_{\alpha_1 j}+\cdots+J_{\alpha_k j})+H}{k_BT}\right) \tag{A5}$$

$$\hat{\mathcal{U}}^k\equiv\sum_{\alpha_1<\cdots<\alpha_k}\frac{[u_{\alpha_1}]_j\cdots[u_{\alpha_k}]_j}{[w_{\alpha_1}]_j\cdots[w_{\alpha_k}]_j}\times\tanh\left(\frac{\sum_{\beta=1}^{N_j}J_{\beta j}-2(J_{\alpha_1 j}+\cdots+J_{\alpha_k j})+H}{k_BT}\right), \tag{A6}$$

so that, for $k=0$,

$$\hat{\mathcal{V}}^0\equiv\tanh\left(\frac{\sum_{\beta=1}^{N_j}J_{\beta j}+H}{k_BT}\right), \tag{A7}$$

$$\hat{\mathcal{U}}^0\equiv\tanh\left(\frac{\sum_{\beta=1}^{N_j}J_{\beta j}+H}{k_BT}\right). \tag{A8}$$

*Present address: Laboratório Nacional de Luz Síncrotron (LNLS), Campinas, SP, 13084-971, Brazil.

[1] E.C. Stoner and E.P. Wohlfarth, Philos. Trans. R. Soc. London, Ser. A **240**, 599 (1948); reprinted in IEEE Trans. Magn. **27**, 3475 (1991).

[2] S.A. Makhlouf, F.T. Parker, F.E. Spada, and A.E. Berkowitz, J. Appl. Phys. **81**, 5561 (1997); R.H. Kodama, S.A. Makhlouf, and A.E. Berkowitz, Phys. Rev. Lett. **79**, 1393 (1997).

[3] W.H. Meiklejohn and C.P. Bean, Phys. Rev. **105**, 904 (1957); S. Banerjee, S. Roy, J.W. Chen, and C. Chakravorty, J. Magn. Magn. Mater. **219**, 45 (2000).

[4] R.H. Kodama, A.E. Berkowitz, E.J. McNiff, Jr., and S. Foner, Phys. Rev. Lett. **77**, 394 (1996); B. Martinez, X. Obradors, Ll. Balcells, A. Rouanet, and C. Monty, *ibid.* **80**, 181 (1997).

[5] R. Prozorov, Y. Yeshurun, T. Prozorov, and A. Gedanken, Phys. Rev. B **59**, 6956 (1999).

[6] W. Wernsdorfer, E.B. Orozco, K. Hasselbach, A. Benoit, D. Mailly, O. Kubo, H. Nakano, and B. Barbara, Phys. Rev. Lett. **79**, 4014 (1997); E. Bonet, W. Wernsdorfer, B. Barbara, A. Benoit, D. Mailly, and A. Thiaville, *ibid.* **83**, 4188 (1999).

[7] M. Jamet, W. Wernsdorfer, C. Thirion, D. Mailly, V. Dupuis, P. Mélinon, and A. Peréz, Phys. Rev. Lett. **86**, 4676 (2001).

[8] J. Shen, R. Skomski, M. Klaua, H. Jenniches, S.S. Manoharan, and J. Kirschner, Phys. Rev. B **56**, 2340 (1997).

[9] M. Plischke and B. Bergersen, *Equilibrium Statistical Physics*, 2nd ed. (World Scientific, Singapore, 1994).
[10] R.J. Glauber, J. Math. Phys. **4**, 294 (1963).
[11] K. Huang, *Statistical Physics*, 2nd ed. (Wiley, New York, 1987).
[12] B.D. Cullit, *Introduction to Magnetic Materials* (Addison-Wesley, London, 1972).
[13] W.H. Meiklejohn, J. Appl. Phys. **33**, 1328 (1962).
[14] R.C. O'Handley, *Modern Magnetic Materials: Principles and Applications* (Wiley New York, 1999).
[15] R. Sappey, E. Vincent, N. Hadacek, F. Chaput, J.P. Boilot, and D. Zins, Phys. Rev. B **56**, 14 551 (1997).